Available online at www.sciencedirect.com
SCIENCE DIRECT®
Comput. Methods Appl. Mech. Engrg. 193 (2004) 575–599
Computer methods in applied mechanics and engineering
www.elsevier.com/locate/cma

# Solution of von-Kármán dynamic non-linear plate equations using a pseudo-spectral method

R.M. Kirby [a], Z. Yosibash [b,*,1]

[a] School of Computing, University of Utah, 84112 Salt Lake City, UT, USA
[b] Division of Applied Mathematics, Brown University, Box F, Providence, RI, 02912, USA

Received 27 May 2003; received in revised form 26 September 2003; accepted 8 October 2003

**Abstract**

The von-Kármán non-linear, dynamic, partial differential system over rectangular domains is solved by the Chebyshev-collocation method in space and the implicit Newmark-β time marching scheme in time. In the Newmark-β scheme, a non-linear fixed point iteration algorithm is employed.

We monitor both temporal and spatial discretization errors based on derived analytical solutions, demonstrating highly accurate approximations. We also quantify the influence of a common modeling assumption which neglects the in-plane inertia terms in the full von-Kármán system, demonstrating that it is justified. A comparison of our steady-state von-Kármán solutions to previous results in the literature and to a three-dimensional high-order finite element analysis is performed, showing an excellent agreement. Other modeling assumptions such as neglecting in-plane quadratic terms in the strain expressions are also addressed.


*Keywords:* von-Kármán plate model; Pseudo-spectral methods; Modeling errors

## 1. Introduction

Plates are viewed in structural engineering practice as three-dimensional components with one of their dimensions, usually denoted by "thickness" ($h$), much smaller compared to the other two dimensions. Due to the complexity of three-dimensional elastic analysis, much attention has been given historically to the derivation of "plate-models", which can be understood as an application of dimensional reduction principles. These plate models are aimed at approximating the three-dimensional problem through a two-dimensional formulation. As the transverse displacement (deflection) in thin plates may be of the same order of magnitude as the plate thickness, it is necessary to formulate the problem to account for large

* Corresponding author.
*E-mail addresses:* kirby@cs.utah.edu (R.M. Kirby), zohar_yosibash@brown.edu, zohary@bgu.ac.il (Z. Yosibash).
[1] Research performed while being on Sabbatical leave from the Department of Mechanical Engineering, Ben-Gurion University, Beer-Sheva, Israel.

0045-7825/$ - see front matter 
doi:10.1016/j.cma.2003.10.013

strains/deflections. The equivalent to the popular plate model of Kirchhoff–Love (derived under the assumption of a small strain situation) is the von-Kármán plate model, which takes into account large deflections. It involves a system of three non-linear time dependent partial differential equations.

The von-Kármán system, although being reduced to a problem over a two-dimensional domain, is still mathematically and numerically very challenging, so that most previous investigations addressed either the time *independent* system, see e.g. [1] and the references therein, or the eigenfrequencies, see e.g. [2]. In many practical engineering problems, such as the fluid–structure interaction problem of a plate embedded in a flow-field, time-dependent von-Kármán solutions are required, thus we address herein the fully non-linear time-dependent von-Kármán system. This system has been investigated by Nath and Kumar [3] (using Chebyshev series), as well as by Gordnier et al. [4,5] (using finite differences and $C^1$ h-version finite element methods). In these works, as in [6], it is assumed *a priori* that terms involving in-plane time derivatives are negligible and are therefore neglected. The neglected terms are the only ones multiplied by the plate thickness, thus neglecting these implies that the solution is thickness independent. Because the system is non-linear and there is no study which quantifies the influence of the in-plane time derivatives on the solution, we herein retain these terms and quantify their influence. Hard-clamped boundary conditions are considered, although other boundary conditions can be easily treated.

In view of the mathematical complexity of the von-Kármán plate model, namely, being a set of three coupled non-linear PDEs involving a biharmonic operator and first and second time derivatives, the numerical solution and the control of both discretization as well as some of the idealization errors are the aim of the present work. Herein we:

- present a high-order spatial discretization based on a pseudo-spectral Chebyshev-collocation method,
- investigate the coupling of the second-order implicit Newmark-β time marching scheme with the spatial pseudo-spectral method so as to provide control of the time-space discretization error. The Newmark-β scheme is applied using a fixed point iteration technique, *without linearization*,
- quantify the idealization error for time dependent solutions introduced by the heuristic assumption of discarding the inertial terms in the momentum equations for the in-plane displacements, and
- compare the steady-state von-Kármán solution (the static elastic non-linear solution) with a three-dimensional elastic non-linear solution in order to quantify the idealization errors introduced when deriving the von-Kármán model from the three-dimensional elasticity equation (discarding the quadratic spatial derivatives of $u$ and $v$, and assuming a Kirchhoff–Love displacement field).

The von-Kármán system, notations, and non-dimensionalization are presented in Section 2. In Section 3 we present two analytical solutions, one for a simplified linear bi-harmonic equation, and the other for the von-Kármán set, based on which we check the convergence rates of our numerical schemes. The spatial discretization by means of the pseudo-spectral Chebyshev-collocation method in conjunction with a temporal discretization using the Newmark-β scheme are presented in Section 4. Numerical experiments and control of spatial and temporal errors are presented in Section 5, whereas some of the modelling errors are discussed in Section 6. The summary, conclusions and open topics of future research are provided in Section 7.

## 2. Notations and formulation

Following [1,6,7] we provide herein the equations describing the von-Kármán plate model made of an isotropic elastic material.

Summation notation is implied (unless otherwise explicitly stated) where summation from 1 to 3 is implied on Latin indices and summation from 1 to 2 is implied on Greek indices. We consider a square plate

of dimensions $a \times a \times h$, with the assumption that $h \ll a$. We denote by $\boldsymbol{x}$ the Cartesian coordinate system $(x_1\, x_2\, x_3)^{\mathrm{T}}$, where the plate thickness is in the $x_3$ direction, and $\boldsymbol{U}(\boldsymbol{x})$ is the displacement vector $(U_1\, U_2\, U_3)^{\mathrm{T}}$ in the corresponding directions (see Fig. 1).

Let $E$ and $v$ be the Young modulus and Poisson ratio of the plate's material, with a density denoted by $\rho$ and a structural viscosity coefficient denoted by $c$. A body force vector, denoted by $\boldsymbol{f}$ can be applied on the plate, where only $f_3 \neq 0$. On the upper and lower surfaces of the plate, we consider traction loading in the $x_3$ direction $g_3^{\pm h/2}$. These are of course prescribed functions of $x_1$, $x_2$ and $t$ alone.

We denote by $E_{ij}(\boldsymbol{U})$ the Green strain tensor (finite strain):

$$E_{ij}(\mathbf{U}) \stackrel{\text{def}}{=} \tfrac{1}{2}(\partial_i U_j + \partial_j U_i + \partial_i U_k \partial_j U_k) \tag{1}$$

where $\partial_i U_j \stackrel{\text{def}}{=} \frac{\partial U_j}{\partial x_i}$. The plate is denoted by $\Omega \times [-\frac{h}{2}, \frac{h}{2}]$ with $\Omega \in \mathbb{R}^2$, and the lateral boundary of the plate is denoted by $\partial\Omega$. The outer normal vector on the boundary $\partial\Omega$ is denoted by $\boldsymbol{n}$, and $(u(x_1, x_2, t) \times v(x_1, x_2, t) w(x_1, x_2, t))^{\mathrm{T}}$ is the displacement vector of the plate mid-surface. The deflection of the mid-surface of the plate is $w$. The in-plane stresses are denoted by $\Sigma_{\alpha\beta}$ and are functions generated by the material properties and $u, v, w$ and are explicitly given in (4).

The model is an approximation of the three-dimensional elastic equations for thin plates, and is derived by asymptotic analysis. The following assumptions are posted in the asymptotic analysis when deriving the von-Kármán model:

- The displacements $\boldsymbol{U}$ are typically of Kirchhoff–Love type, i.e. can be generated from the mid-surface displacement vector as follows:

$$U_1 = u - x_3 \partial_1 w, \quad U_2 = v - x_3 \partial_2 w, \quad U_3 = w \tag{2}$$

  This is the first source of idealization errors, namely the assumptions on the functional representation of the displacement fields in the $x_3$ direction.
- Only the terms involving $w$ are retained in the quadratic terms in (1).
- Terms associated with the rotational inertia will be neglected.
- The body forces are of the form $\boldsymbol{f} = (0\ 0\ f_3)^{\mathrm{T}}$.
- Shear stresses on $x_3 = \pm h/2$ are negligible.

Some derivations also assume that the accelerations in $x_\alpha$ directions are negligible, however, we will treat these inertial terms in our formulation also.

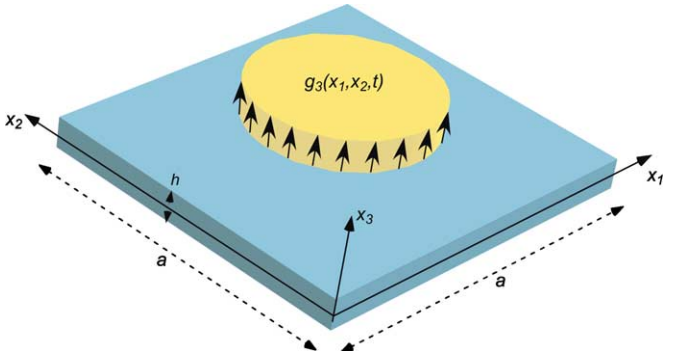


Fig. 1. Notations for plate of interest.

Let us denote by $E^{\circ}_{\alpha\beta}$ the (symmetric) "in-plane Green strain" defined by:

$$E^{\circ}_{\alpha\beta} = \frac{1}{2}\begin{cases} (2\partial_1 u + (\partial_1 w)^2) & \alpha = \beta = 1, \\ (2\partial_2 v + (\partial_2 w)^2) & \alpha = \beta = 2, \\ \frac{1}{2}(\partial_2 u + \partial_1 v + \partial_1 w \partial_2 w) & \text{otherwise.} \end{cases} \tag{3}$$

By the definition of the Green strain as in (3), an idealization error is introduced, assuming the terms of the form $\partial_i u \partial_j u$ and of the form $\partial_i v \partial_j v$ are negligible with respect to $\partial_1 w \partial_2 w$.

The "in-plane stresses" $\Sigma_{\alpha\beta}$ are connected to the mid-plane displacements by:

$$\Sigma_{\alpha\beta} \overset{\text{def}}{=} hE\left[\frac{\nu}{1-\nu^2}\delta_{\alpha\beta}E^{\circ}_{\theta\theta} + \frac{1}{1+\nu}E^{\circ}_{\alpha\beta}\right], \tag{4}$$

$$= \begin{cases} \dfrac{hE}{2(1+\nu)}\left\{\dfrac{\nu}{1-\nu}[2\partial_1 u + 2\partial_2 v + (\partial_1 w)^2 + (\partial_2 w)^2] + 2\partial_1 u + (\partial_1 w)^2\right\} & \alpha = \beta = 1, \\ \dfrac{hE}{2(1+\nu)}\left\{\dfrac{\nu}{1-\nu}[2\partial_1 u + 2\partial_2 v + (\partial_1 w)^2 + (\partial_2 w)^2] + 2\partial_2 v + (\partial_2 w)^2\right\} & \alpha = \beta = 2, \\ \dfrac{hE}{2(1+\nu)}\{\partial_2 u + \partial_1 v + \partial_1 w \partial_2 w\} & \text{otherwise.} \end{cases} \tag{5}$$

With the above definitions, the system of three PDEs for the computation of the three unknown functions for any $(x_1, x_2) \in \Omega$ is [1,7]:

$$h\rho\ddot{w} - \rho\frac{h^3}{12}\nabla^2\ddot{w} + hc\dot{w} + D\nabla^4 w - \partial_\alpha(\Sigma_{\alpha\beta}\partial_\beta w) = \int_{-\frac{h}{2}}^{\frac{h}{2}} f_3 \,\mathrm{d}x_3 + g_3^{\frac{h}{2}} + g_3^{-\frac{h}{2}}, \tag{6}$$

$$h\rho\ddot{u} + hc\dot{u} - \partial_\alpha\Sigma_{1\alpha} = 0, \tag{7}$$

$$h\rho\ddot{v} + hc\dot{v} - \partial_\alpha\Sigma_{2\alpha} = 0, \tag{8}$$

where $D \overset{\text{def}}{=} \frac{Eh^3}{12(1-\nu^2)}$ is the flexural rigidity.

**Remark 1.** One has to find three unknown functions $u(x_1, x_2, t)$, $v(x_1, x_2, t)$, $w(x_1, x_2, t)$, over the two-dimensional domain $\Omega$, which describe the displacements of the mid-surface of the plate.

**Remark 2.** The second term in (6) representing rotational inertia is frequently neglected as we shall do too, but the other terms are retained in our formulation, although these are neglected in other publications also. The last term in the LHS of Eqs. (6)–(8) is a non-linear term in the formulation since it involves higher order terms, and also generates the coupling between the various unknown functions. Observe that this is the reason why one cannot split the expression for the energy into pure bending energy and pure tension energy!

The von-Kármán equations have to be complimented by appropriate boundary conditions. Two of the commonly used boundary conditions in engineering practice are:

- "Soft-clamped" boundary conditions:

$$\left.\begin{array}{l} U_3 = 0 \\ U_1 \ \& \ U_2 \text{ independent of } x_3 \end{array}\right\} \text{ on } \partial\Omega \times \left[-\frac{h}{2}, \frac{h}{2}\right] \tag{9}$$

which imply the following boundary conditions for the functions $u, v, w$:

$$w = \partial_n w = 0 \quad \text{on } \partial\Omega, \tag{10}$$

$$\Sigma_{\alpha\beta} n_\beta = h_\beta \quad \text{on } \partial\Omega, \tag{11}$$

where $h_\beta$ are averaged "in-plane" traction boundary conditions on the lateral boundary of the domain.

- "Hard-clamped" boundary conditions:

$$U_1 = U_2 = U_3 = 0 \quad \text{on } \partial\Omega \times \left[-\frac{h}{2}, \frac{h}{2}\right], \tag{12}$$

which imply the following boundary conditions for the functions $u, v, w$:

$$u = v = w = \partial_n w = 0 \quad \text{on } \partial\Omega. \tag{13}$$

Assuming no body forces ($f_3 = 0$), then (6)–(8) in terms of the three displacement functions can be expressed as:

$$h(\rho\ddot{w} + c\dot{w}) + D\nabla^4 w - \frac{12D}{h^2}\left[\left(u_{,1} + \frac{1}{2}w_{,1}^2\right)(w_{,11} + \nu w_{,22}) + \left(v_{,2} + \frac{1}{2}w_{,2}^2\right)(w_{,22} + \nu w_{,11}) + (1-\nu)(v_{,1} + u_{,2} + w_{,1}w_{,2})w_{,12}\right] = g_3^{\frac{h}{2}} + g_3^{-\frac{h}{2}} \stackrel{\text{def}}{=} g(x_1, x_2, t), \tag{14}$$

$$h(\rho\ddot{u} + c\dot{u}) - \frac{6D}{h^2}[2u_{,11} + (1+\nu)v_{,12} + (1-\nu)u_{,22} + 2w_{,1}w_{,11} + (1+\nu)w_{,2}w_{,12} + (1-\nu)w_{,1}w_{,22}] = 0, \tag{15}$$

$$h(\rho\ddot{v} + c\dot{v}) - \frac{6D}{h^2}[2v_{,22} + (1+\nu)u_{,12} + (1-\nu)v_{,11} + 2w_{,2}w_{,22} + (1+\nu)w_{,1}w_{,12} + (1-\nu)w_{,2}w_{,11}] = 0. \tag{16}$$

The boundary conditions, denoted by "hard clamped" which complement the system of PDEs are considered in the present paper, although "soft-clamped" boundary conditions are a straight-forward generalization of the methods presented.

### 2.1. Non-dimensionalization of (14)–(16)

Following [3] we perform the following change of variables:

$$\hat{u} = \frac{(a/2)u}{h^2}, \quad \hat{v} = \frac{(a/2)v}{h^2}, \quad \hat{w} = \frac{w}{h}, \quad \hat{x}_1 = \frac{x_1}{(a/2)}, \quad \hat{x}_2 = \frac{x_2}{(a/2)}, \quad \hat{t} = t\sqrt{\frac{D}{\rho h (a/2)^4}},$$

$$\hat{g} = \frac{g(a/2)^4}{Dh}, \quad \hat{h} = \frac{h}{(a/2)}, \quad \hat{c} = c\sqrt{\frac{(a/2)^4 h}{\rho D}}.$$

With the above set of non-dimensional variables, Eqs. (14)–(16) can be written in non-dimensional form:

$$\hat{w}_{,\hat{t}\hat{t}} + \hat{c}\hat{w}_{,\hat{t}} + \hat{\nabla}^4\hat{w} - 12[(\hat{u}_{,\hat{1}} + \tfrac{1}{2}\hat{w}_{,\hat{1}}^2)(\hat{w}_{,\hat{1}\hat{1}} + \nu\hat{w}_{,\hat{2}\hat{2}}) + (\hat{v}_{,\hat{2}} + \tfrac{1}{2}\hat{w}_{,\hat{2}}^2)(\hat{w}_{,\hat{2}\hat{2}} + \nu\hat{w}_{,\hat{1}\hat{1}}) + (1-\nu)(\hat{v}_{,\hat{1}} + \hat{u}_{,\hat{2}} + \hat{w}_{,\hat{1}}\hat{w}_{,\hat{2}})\hat{w}_{,\hat{1}\hat{2}}] = \hat{g}_3, \tag{17}$$

$$\frac{\hat{h}^2}{6}(\hat{u}_{,\hat{t}\hat{t}} + \hat{c}\hat{u}_{,\hat{t}}) - [2\hat{u}_{,\hat{1}\hat{1}} + (1+\nu)\hat{v}_{,\hat{1}\hat{2}} + (1-\nu)\hat{u}_{,\hat{2}\hat{2}} + 2\hat{w}_{,\hat{1}}\hat{w}_{,\hat{1}\hat{1}} + (1+\nu)\hat{w}_{,\hat{2}}\hat{w}_{,\hat{1}\hat{2}} + (1-\nu)\hat{w}_{,\hat{1}}\hat{w}_{,\hat{2}\hat{2}}] = 0, \tag{18}$$

$$\frac{\hat{h}^2}{6}(\hat{v}_{,\hat{t}\hat{t}} + \hat{c}\hat{v}_{,\hat{t}}) - [2\hat{v}_{,\hat{2}\hat{2}} + (1+\nu)\hat{u}_{,\hat{1}\hat{2}} + (1-\nu)\hat{v}_{,\hat{1}\hat{1}} + 2\hat{w}_{,\hat{2}}\hat{w}_{,\hat{2}\hat{2}} + (1+\nu)\hat{w}_{,\hat{1}}\hat{w}_{,\hat{1}\hat{2}} + (1-\nu)\hat{w}_{,\hat{2}}\hat{w}_{,\hat{1}\hat{1}}] = 0. \tag{19}$$

The boundary conditions, denoted by "hard clamped" which complement the system of PDEs are:

$$\hat{u} = \hat{v} = \hat{w} = \partial_n \hat{w} = 0 \quad \text{on } \partial\Omega. \tag{20}$$

**Remark 3.** The first two time dependent terms in (18) and (19) are of order $\hat{h}^2$ compared to the order one terms in the rest of the equations, so are commonly neglected (see [1,3,5] for example). This set of equations will be denoted by *simplified von-Kármán* set, as opposed to the *full von-Kármán* system (17)–(19). The simplified von-Kármán system considerably simplifies its numerical treatment as one is left with one prognostic equation (17) with two "constraint equations", a set which is much easier to solve. Nath and Kumar [3] and Gordnier and Visbal [5] considered the simplified von-Kármán set of equations.

**Remark 4.** Notice that Nath and Kumar [3] have an error in their Eqs. (1) and (B.1), where instead of $(1-\nu)$ they mistakenly have $(1-\nu^2)$. This may result in the slightly difference when compared to the work by Timoshenko. Furthermore, the non-dimensionalization of the viscosity term in their (4) has an error, and $\rho$ should be in the denominator instead of the numerator.

## 3. Analytic solutions for a bi-harmonic equation and a special case of the full von-Kármán system

To verify the numerical code and the proper treatment of boundary conditions and still obtain the spectral convergence expected of the Chebyshev-collocation method, we introduce the following simple bi-harmonic example problem for which an analytical solution is available.

*Linear bi-harmonic problem for verification of the pseudo-spectral method*: Consider the linear bi-harmonic equation:

$$\frac{\partial^2 u(x_1,x_2,t)}{\partial t^2} = -\nabla^4 u(x_1,x_2,t) + g(x_1,x_2,t) \quad \text{on} \quad \Omega = (0,1)\times(0,1) \tag{21}$$

with the following boundary conditions:

$$\begin{aligned} &u(0,x_2,t) = u(1,x_2,t) = u(x_1,0,t) = u(x_1,1,t) = 0,\\ &u_{,1}(0,x_2,t) = u_{,1}(1,x_2,t) = u_{,2}(x_1,0,t) = u_{,2}(x_1,1,t) = 0, \end{aligned} \tag{22}$$

and with the following initial conditions:

$$u(x_1,x_2,0) = u_{,t}(x_1,x_2,0) = 0. \tag{23}$$

For a given forcing function $g(x_1,x_2,t)$:

$$\begin{aligned} g(x_1,x_2,t) = -\mathrm{e}^{-t}\{&(2-4t+t^2)\sin^2(\pi x_2) - 8t^2\pi^4[\cos(2\pi x_1)\sin^2(\pi x_2)\\ &+ \cos(2\pi x_2)\sin^2(\pi x_1) - \cos(2\pi x_1)\cos(2\pi x_2)]\}, \end{aligned} \tag{24}$$

one obtains an exact solution given by:

$$u(x_1,x_2,t) = t^2\mathrm{e}^{-t}\sin^2(\pi x_1)\sin^2(\pi x_2).$$

This example serves for verification of the convergence rates when using the Chebyshev-collocation method and the proper implementation of boundary conditions.

*The full von-Kármán system with an analytic solution*: In this paper we consider a plate having the dimensions $a/2 = half\ plate\ length = half\ plate\ width = 1$, with its left lower corner located at $(\hat{x}_1, \hat{x}_2) = (0,0)$. To check the temporal and spatial convergence rates for a non-linear system, consider von-Kármán equations (17)–(19) with $\hat{c} = 0$, $\nu = 0.3$, clamped boundary conditions, initial displacements and velocities being zero, and a non-homogeneous right-hand side given by:

$$\begin{aligned}
\text{RHS of (17)} = {} & e^{-3\hat{t}}\hat{t}\{-0.36825441267825e^{\hat{t}}\hat{t}^5\cos^3\pi\hat{x}_1\sin^3\pi\hat{x}_2 \\
& - 1.1968268412043\hat{t}^8\cos^4\pi\hat{x}_1\sin^2\pi\hat{x}_1\sin^6\pi\hat{x}_2 \\
& + e^{\hat{t}}\hat{t}^5\cos\pi\hat{x}_1\sin^2\pi\hat{x}_1\sin\pi\hat{x}_2(-0.626032501553018\cos^2\pi\hat{x}_2 \\
& + 0.478730736481719\sin^2\pi\hat{x}_2) + \hat{t}^2\cos^2\pi\hat{x}_1[-98.9577178047726e^{2\hat{t}}\sin^2\pi\hat{x}_2 \\
& - 0.626032501553018e^{\hat{t}}\hat{t}^3\cos\pi\hat{x}_2\sin\pi\hat{x}_1\sin^2\pi\hat{x}_2 + 1.55587489356559\hat{t}^6\sin^4\pi\hat{x}_1\sin^6\pi\hat{x}_2 \\
& + \cos^2\pi\hat{x}_2(49.4788589023863e^{2\hat{t}} - 4.0692112600946\hat{t}^6\sin^4\pi\hat{x}_1\sin^4\pi\hat{x}_2)] \\
& + \sin^2\pi\hat{x}_1[-0.36825441267825e^{\hat{t}}\hat{t}^5\cos^3\pi\hat{x}_2\sin\pi\hat{x}_1 \\
& + 148.5000703430931e^{2\hat{t}}(0.00256539821648 - 0.00256539821648\hat{t} + \hat{t}^2)\sin^2\pi\hat{x}_2 \\
& + 0.478730736481719e^{\hat{t}}\hat{t}^5\cos\pi\hat{x}_2\sin\pi\hat{x}_1\sin^2\pi\hat{x}_2 \\
& - 1.1968268412043\hat{t}^8\cos^4\pi\hat{x}_2\sin^4\pi\hat{x}_1\sin^2\pi\hat{x}_2 \\
& + \cos^2\pi\hat{x}_2(-98.9577178047726e^{2\hat{t}}\hat{t}^2 + 1.55587489356559\hat{t}^8\sin^4\pi\hat{x}_1\sin^4\pi\hat{x}_2)]\},
\end{aligned}$$

$$\begin{aligned}
\text{RHS of (18)} = {} & e^{-2\hat{t}}\hat{t}\Bigg\{0.007793937203257e^{\hat{t}}\left[26.647931882941262\hat{t}^2 + \frac{\hat{h}^2}{6}(6 - 6\hat{t} + \hat{t}^2)\right]\sin\pi\hat{x}_1\sin\pi\hat{x}_2 \\
& - \hat{t}^5\cos^3\pi\hat{x}_1\sin\pi\hat{x}_1\sin^4\pi\hat{x}_2 + \cos\pi\hat{x}_1[-0.1e^{\hat{t}}\hat{t}^2\cos\pi\hat{x}_2 - 1.65\hat{t}^5\cos^2\pi\hat{x}_2\sin^3\pi\hat{x}_1\sin^2\pi\hat{x}_2 \\
& + 1.35\hat{t}^5\sin^3\pi\hat{x}_1\sin^4\pi\hat{x}_2]\Bigg\},
\end{aligned}$$

$$\begin{aligned}
\text{RHS of (19)} = {} & e^{-2\hat{t}}\hat{t}\Bigg\{-0.1e^{\hat{t}}\hat{t}^2\cos\pi\hat{x}_1\cos\pi\hat{x}_2 - 1.65\hat{t}^5\cos^2\pi\hat{x}_1\cos\pi\hat{x}_2\sin^2\pi\hat{x}_1\sin^3\pi\hat{x}_2 \\
& + 0.007793937203257e^{\hat{t}}\left[26.647931882941272\hat{t}^2 + \frac{\hat{h}^2}{6}(6 - 6\hat{t} + \hat{t}^2)\right]\sin\pi\hat{x}_1\sin\pi\hat{x}_2 \\
& + \hat{t}^5\sin^4\pi\hat{x}_1(-\cos^3\pi\hat{x}_2\sin\pi\hat{x}_2 + 1.35\cos\pi\hat{x}_2\sin^3\pi\hat{x}_2)\Bigg\}.
\end{aligned}$$

The above RHS was derived by substituting into Eqs. (17)–(19) the following assumed solutions:

$$\hat{u} = 0.007793937203257\hat{t}^3e^{-\hat{t}}\sin\pi\hat{x}_1\sin\pi\hat{x}_2, \tag{25}$$

$$\hat{v} = 0.007793937203257\hat{t}^3e^{-\hat{t}}\sin\pi\hat{x}_1\sin\pi\hat{x}_2, \tag{26}$$

$$\hat{w} = 0.0634936359342\hat{t}^3e^{-\hat{t}}\sin^2\pi\hat{x}_1\sin^2\pi\hat{x}_2. \tag{27}$$

Although the coefficients of the assumed solutions above look intriguing, they have been selected so as to produce expressions which are relatively simple in the RHS of (17)–(19).

If one considers the simplified von-Kármán system, *without the first two time derivatives terms in* (17)–(19), and $\hat{c} = 0$, $\nu = 0.3$, clamped boundary conditions, and initial displacements and velocities zero, then (25)–(27) is still its exact solution if the RHS of Eqs. (18) and (19) are changed to:

$$\begin{aligned}\text{RHS of } (18) = {} & \mathrm{e}^{-2\hat{t}}\hat{t}^3\{0.20769230769231\mathrm{e}^{\hat{t}}\sin\pi\hat{x}_1\sin\pi\hat{x}_2 - \hat{t}^3\cos^3\pi\hat{x}_1\sin\pi\hat{x}_1\sin^4\pi\hat{x}_2 \\ & + \cos\pi\hat{x}_1[-0.1\mathrm{e}^{\hat{t}}\cos\pi\hat{x}_2 - 1.65\hat{t}^3\cos^2\pi\hat{x}_2\sin^3\pi\hat{x}_1\sin^2\pi\hat{x}_2 + 1.35\hat{t}^3\sin^3\pi\hat{x}_1\sin^4\pi\hat{x}_2]\},\end{aligned}$$

$$\begin{aligned}\text{RHS of } (19) = {} & \mathrm{e}^{-2\hat{t}}\hat{t}^3\{-0.1\mathrm{e}^{\hat{t}}\cos\pi\hat{x}_1\cos\pi\hat{x}_2 - 1.65\hat{t}^3\cos^2\pi\hat{x}_1\cos\pi\hat{x}_2\sin^2\pi\hat{x}_1\sin^3\pi\hat{x}_2 + \sin\pi\hat{x}_1\sin\pi\hat{x}_2 \\ & \times[0.20769230769231\mathrm{e}^{\hat{t}} - \hat{t}^3\cos^3\pi\hat{x}_2\sin^3\pi\hat{x}_1 + 1.35\hat{t}^3\cos\pi\hat{x}_2\sin^3\pi\hat{x}_1\sin^2\pi\hat{x}_2]\}.\end{aligned}$$

The problems with analytic solutions presented herein are used for verifying the spectral and temporal discretization schemes introduced in the next section.

## 4. Numerical formulation

We solve numerically the non-dimensional form of the von-Kármán plate model using a pseudo-spectral Chebyshev-collocation method [8,9] for the spatial discretization and the Newmark-β scheme [10] for integration in time. In this section we elaborate on each of these components of our work.

Pseudo-spectral methods [8,9] as well as high-order finite element methods [11,12] were shown to be efficient for spatial-discretization, yielding in "exponential (spectral) converge rates", and have been used in [2,3] for the solution of variants of the von-Kármán system. Due to the bi-harmonic operator, the finite-element formulation requires $C^1$ continuous elements, thus considerably affects the computational complexity. The Chebyshev-collocation method on the other hand can easily treat the non-linear terms and is a natural choice for quadrilateral domains, and thus has been adopted in the present work (differences compared to [3] with respect to the handling of the boundary conditions and the non-linear terms will be explained in the next section).

### 4.1. Spatial discretization

As the spatial discretization, we chose to use a Chebyshev-collocation method as described in [8,9]. To explain the methodology and for ease of presentation, we use the following simplified one-dimensional linear diffusion problem (after which the extension of this methodology to two-dimensions and to non-linear problems will be discussed):

$$\frac{\partial u(x,t)}{\partial t} = \nu\frac{\partial^2 u(x,t)}{\partial x^2}$$

on the interval $[0,a]$ with initial condition $u(x,t=0) = u_0(x)$ (a given smooth function) and boundary conditions $u(0,t) = u(a,t) = 0$. This equation is chosen merely as a simple example partial differential equation commonly seen in elementary numerical analysis texts. We begin by discretizing the interval $[0,a]$ using a mapping of the Chebyshev–Lobatto point distribution given on $[-1,1]$ as $x_j = \cos(j\pi/N), j = 0,\ldots,N$. In a collocation method we seek an approximate solution $\tilde{u}(x,t)$ which satisfied the differential equation exactly at the grid points. Hence we seek an approximate solution $\tilde{u}(x,t)$ which "collocates" the partial differential equation, that is, we try to find $\tilde{u}(x,t)$ such that:

$$\frac{\partial \tilde{u}(x_j,t)}{\partial t} = \nu\frac{\partial^2 \tilde{u}(x_j,t)}{\partial x^2}$$

for all collocation points $x_j, j = 0, \ldots, N$. If we assume that we evaluate the solution of our system at these points, we can form an $N$th order approximating interpolant of the solution. We approximate derivatives of the solution by computing derivatives of the approximating interpolating polynomial. Mathematically, the operation of computing the derivative of the interpolating polynomial can be formulated as pre-multiplying the collocated data by a collocation derivative matrix $\mathbf{D}$ (as given in [9, p. 53]). Higher-order derivatives can be obtained through successive application of the matrix operator $\mathbf{D}$. Thus, if we define our solution vector as $\vec{u} = (\tilde{u}(x_0, t), \ldots, \tilde{u}(x_N, t))^{\mathrm{T}}$ and we substitute continuous derivative with the discrete collocation derivative operator $\mathbf{D}$, our problem now becomes a matter of solving the following linear system of ordinary differential equations:

$$\frac{\partial \hat{u}}{\partial t} = \nu \mathbf{D}^2 \vec{u}.$$

Dirichlet boundary conditions can be handled strongly by setting $\tilde{u}(x_0, t) = \tilde{u}(x_N, t) = 0$. To extend this to two-dimensions, we discretize our two-dimensional domain using the tensor product of the one-dimensional Chebyshev–Lobatto point distribution. Two-dimensional derivative approximations are accomplished by successive application of one-dimensional derivative operations. Mathematically this equates to constructing a two-dimensional derivative operator as the Kronecker sum of the one-dimensional derivative operators.

Using the methodology as discussed above, Eqs. (17)–(19) are solved in a *point-wise* fashion where spatial derivative operators are replaced by the appropriate discrete collocation derivative operators. This form of discretization allows for easy implementation of the non-linear terms; non-linearities are handled by point-wise evaluation at the collocation points. This approach was used by Nath and Kumar [3] for solving the von-Kármán system. They, however, did not chose to solve the full non-linear system directly (and hence did not collocate the non-linear terms directly). Instead, they first write the von-Kármán system in terms of Chebyshev sums, then *linearize* the system before collocating their equations. In this work, we do not linearize the equations, but instead we collocate the full non-linear system directly.

In the example above, we discussed simple Dirichlet boundary conditions of a second-order spatial operator. For collocation methods of this type, special care must be taken so that boundary conditions associated with a fourth-order differential operator (like the bi-harmonic operator in the von-Kármán equations) are properly handled. In general, there are two basic approaches which may be used to satisfy boundary conditions when using pseudo-spectral collocation methods:

(1) Restrict attention to polynomial interpolants that (automatically) satisfy the boundary conditions; or
(2) Do not restrict the interpolants but rather add additional equations to enforce boundary conditions.

Nath and Kumar [3] applied the second approach which, in their case, led to an over-specified system of equations. Hence their algorithm required the addition of a projection method for determining the solution. We have chosen the first approach upon which we will now elaborate.

The complication of satisfying simultaneously the boundary conditions on the function itself *and* its normal derivative, can be accomplished through a careful modification of the fourth-derivative collocation operator [9]. This modification consists of restricting our polynomial interpolants of order $N$ to be of the form (in one-dimension) $p(x) = (1 - x^2)q(x)$ where $q(x)$ is a polynomial of degree $N - 2$ such that $q(\pm 1) = 0$. Observe that the polynomial $p(x)$ has been devised so that $p(\pm 1) = 0$ *and* $\partial_x p(\pm 1) = 0$. This restriction equates to constraining our polynomial search space to only those polynomial interpolants having roots at $x = \pm 1$ with a multiplicity of two or higher.

Given that our polynomial interpolant $p(x)$ is defined as just previously given, we can construct an matrix operator $\mathbf{D}_4$ which approximates the fourth-derivative *and* satisfies both $p(\pm 1) = \partial_x p(\pm 1) = 0$ conditions as follows:

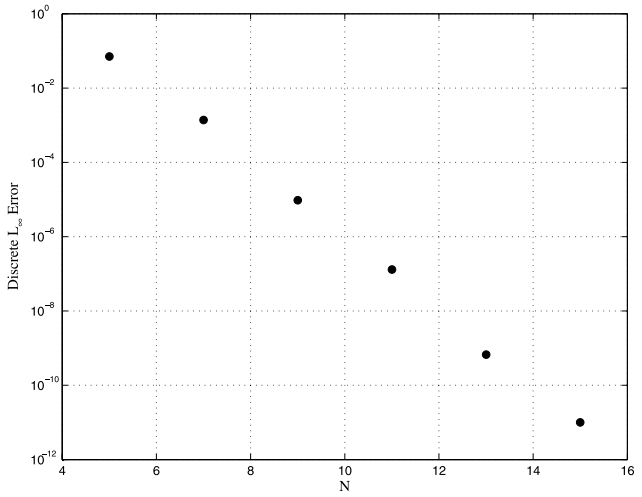


Fig. 2. Discrete $L_\infty$ error versus the number of grid points used per direction in the Chebyshev collocation scheme. Data shown is taken at $t = 1$ with $\Delta t = 10^{-6}$.

$$\mathbf{D}_4 = (\mathbf{A}\mathbf{D}^4 - 8\mathbf{B}\mathbf{D}^3 - 12\mathbf{D}^2)\mathbf{A}^{-1}, \tag{28}$$

where $\mathbf{A} = A_{ij} = (1 - x_j^2)\delta_{ij}$ and $\mathbf{B} = B_{ij} = x_j\delta_{ij}$, the set $\{x_j\}$ is the Chebyshev–Lobatto point distribution on $[-1, 1]$, and $\mathbf{D}$ is the one-dimensional Chebyshev-collocation derivative operator (see [13] for details).

To verify that we properly satisfy the boundary conditions and that we still obtain the spectral convergence expected of the Chebyshev-collocation method, we solved the linear bi-harmonic equation (21), subjected to the boundary conditions and initial conditions (22) and (23) and the forcing function given by (24). We use the Chebyshev-collocation method with boundary condition modification as described above using the second-order Newmark-β scheme (to be described in the following section).

In Fig. 2 we plot the discrete $L_\infty$ error defined as

$$L_\infty \stackrel{\text{def}}{=} \max_{x_i, x_j} |u_{\text{approx}}(x_i, x_j) - u_{\text{exact}}(x_i, x_j)| \tag{29}$$

taken over the collocation point grid $(x_i, x_j)$ versus the number of points used per direction evaluated at the time $t = 1$. A time step of $\Delta t = 10^{-6}$ was used (so that given the second-order convergence in time of our time integrator we should expect time dicretization errors on the order of $10^{-12}$ and hence spatial errors should dominate); the exact solution was used to initialize the time integrator. Observe in Fig. 2 that on a log-linear plot a straight line is obtained indicating an exponential convergence rate to the exact solution with increasing $N$.

This example serves to demonstrate the correctness of both the Chebyshev-collocation method and the boundary condition implementation used for a bi-harmonic PDE.

### 4.2. Temporal discretization

To discretize the von-Kármán system in time, we have chosen to employ the Newmark-β scheme [10]. For our first attempt we used the fully explicit form of the Newmark-β scheme given by the following expression:

$$\frac{\mathrm{d}^2 u}{\mathrm{d}t^2} = \frac{u^{n+1} - 2u^n + u^{n-1}}{\Delta t^2} + \mathcal{O}(\Delta t^2).$$

Because of the small stability region of this explicit scheme coupled with the large "wave speeds" associated with Eqs. (18) and (19) we found the time step required to meet the CFL condition overly restrictive. We hence chose to use the average acceleration variant of the Newmark-β scheme (with Newmark parameters $\gamma = \frac{1}{2}$ and $\beta = \frac{1}{4}$) which also exhibits second-order convergence in time and is unconditionally stable under linear analysis.

The variant of the Newmark-β scheme which we employed can be algorithmically described as follows. Assume one is given the equation:

$$m\ddot{u} + c\dot{u} + ku = g, \tag{30}$$

where the forcing $g$ may be a function of the solution $u$. Discretizing in time we obtain the expressions at time level $n$ and $n+1$ respectively:

$$\begin{aligned} &m\ddot{u}_n + c\dot{u}_n + ku_n = g_n, \\ &m\ddot{u}_{n+1} + c\dot{u}_{n+1} + ku_{n+1} = g_{n+1}. \end{aligned} \tag{31}$$

The average acceleration variant of the Newmark-β scheme (see [10]) are given by the following time difference equations:

$$\begin{aligned} \dot{u}_{n+1} &= \dot{u}_n + \frac{\Delta t}{2}(\ddot{u}_n + \ddot{u}_{n+1}) \\ u_{n+1} &= u_n + \Delta t\dot{u}_n + \frac{(\Delta t)^2}{4}(\ddot{u}_n + \ddot{u}_{n+1}), \end{aligned} \tag{32}$$

where the local truncation error of these equations is $\mathcal{O}(\Delta t^2)$. We can now combine Eqs. (31) and (32) to yield the following equation for the solution $u$ at time level $n+1$ given information at time level $n$ and the forcing function $g$ at time level $n+1$:

$$\left(\frac{4m}{(\Delta t)^2} + \frac{2c}{\Delta t} + k\right)u_{n+1} = g_{n+1} + m\left(\frac{4}{(\Delta t)^2}u_n + \frac{4}{\Delta t}\dot{u}_n + \ddot{u}_n\right) + c\left(\frac{2}{\Delta t}u_n + \dot{u}_n\right). \tag{33}$$

To demonstrate the second-order temporal convergence rate of this scheme, we revisit the bi-harmonic equation (see Eqs. (21)–(23) presented in the previous section. Observe that in solving Eq. (21) we have a right-hand-side term $g_{n+1}$ which is a function of the solution $u_{n+1}$. Discretizing Eq. (21) in the form given in Eq. (33) yields the following expression:

$$\left(\frac{4}{(\Delta t)^2}\right)\left(1 + \frac{(\Delta t)^2}{4}\nabla^4\right)u_{n+1}(x_1, x_2) = g_{n+1}(x_1, x_2) + \left(\frac{4}{(\Delta t)^2}u_n + \frac{4}{\Delta t}\dot{u}_n + \ddot{u}_n\right).$$

After substituting in the spatial discretization operators discussed previously, we arrive at a set of linear equations for which to solve. Given the linearity of the system we can directly invert the operator on the left hand side to yield the solution $u_{n+1}$ in terms of the solution $u_n$ and the forcing $g(x_1, x_2, t)$ evaluated at the new time level $t_{n+1}$. In Fig. 3 we plot the discrete $L_\infty$ error (as defined in Eq. (29)) versus time step for a spatial discretization of $N = 21$ points per collocated direction. Observe that on a log–log plot we obtain a straight line of slope 2.0 indicating that second-order convergence has been achieved.

Unlike the example problem given above, the von-Kármán model which we are solving is not linear, and hence direct inversion cannot be used. There exist two general approaches to solving this type of non-linear system:

(1) Linearize the equations about some state and use sub-iteration of the linearized problem to obtain to the solution of the non-linear problem, or
(2) Solve directly the non-linear problem, making no linearizing assumptions.

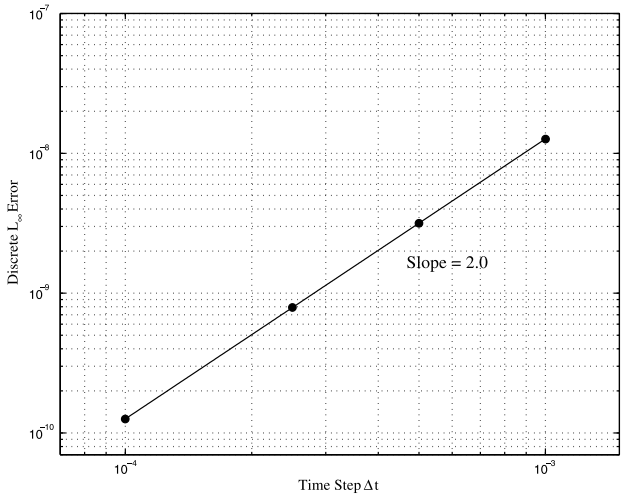


Fig. 3. Discrete $L_\infty$ error versus the time step $\Delta t$. The comparison is done at time $t = 1$.

The first of these two approaches was used by Nath and Kumar [3] and Gordnier and Visbal [5]. We have chosen the second approach, which does not allow us to use direct inversion of a linear system; however, following the second approach we also have no linearization considerations.

To solve the non-linear system given in Eqs. (17)–(19) directly, we employ the fixed point method of solving a non-linear system of equations [14]. This can be understood as follows. First, define the solution vector as $\vec{u} = (\hat{u}(x_1, x_2, t), \hat{v}(x_1, x_2, t), \hat{w}(x_1, x_2, t))^{\mathrm{T}}$. We can thus re-write Eqs. (17)–(19) as:

$$\frac{\partial^2 \vec{u}}{\partial \hat{t}^2} + \hat{c}\frac{\partial \vec{u}}{\partial \hat{t}} = G(\vec{u}),$$

where we have grouped all the non-linear terms and forcing terms into the expression $G(\vec{u})$. We now discretize this system in time using Eq. (33) to obtain:

$$\left(\frac{4}{(\Delta t)^2} + \frac{2\hat{c}}{\Delta t}\right)\vec{u}_{n+1} = G(\vec{u}_{n+1}) + \left(\frac{4}{(\Delta t)^2}\vec{u}_n + \frac{4}{\Delta t}\dot{\vec{u}}_n + \ddot{\vec{u}}_n\right) + \hat{c}\left(\frac{2}{\Delta t}\vec{u}_n + \dot{\vec{u}}_n\right).$$

The equation above can easily be re-cast in the following form:

$$\vec{u}_{n+1} = \widetilde{G}(\vec{u}_{n+1}), \tag{34}$$

where we have grouped all the terms involving information at time level $n$ and all non-linear and forcing terms into the expression $\widetilde{G}$. Written in this form, we see that this is a candidate for the fixed point method. Henceforth, for all our von-Kármán tests, we employ this combination of the Newmark-β scheme with the fixed point iteration method.

In the case of the simplified von-Kármán equations, we can still use the fixed point iteration to solve the system. Unlike linearization schemes which require sub-iteration, we can incorporate the constraining system into the fixed point iterative scheme as follows. With $\hat{h} = 0$, Eqs. (18) and (19) can be re-written in the form:

$$\mathscr{L}\begin{pmatrix}\hat{u}\\ \hat{v}\end{pmatrix} = \mathscr{N}_{uv}(\hat{w}), \tag{35}$$

where $\mathscr{L}$ is a linear differential operator and $\mathscr{N}_{uv}$ is a non-linear operator operating on $\hat{w}$. Since $\mathscr{L}$ is a linear operator, it can be inverted directly. Combining Eq. (35) for $\hat{u}$ and $\hat{v}$ with a time discretization for $\hat{w}$ as in Eq. (33), we obtain a system of the form given in Eq. (34) (with the $\widetilde{G}$ being different, however, than in the full von-Kármán case). The new fixed point system now becomes

$$\begin{pmatrix}\hat{u}\\ \hat{v}\\ \hat{w}\end{pmatrix}_{n+1} = \begin{pmatrix}\mathscr{L}^{-1}\mathscr{N}_{uv}(\hat{w}_{n+1})\\ \mathscr{N}_{w}(\vec{u}_{n+1})\end{pmatrix},$$

where $\mathscr{N}_w(\vec{u})$ denotes a grouping of all the terms involving information at time level $n$ and all non-linear and forcing terms for the time marching of the $\hat{w}$ displacement.

To demonstrate the spatial convergence properties of our numerical scheme, we solved both full and simplified von-Kármán systems with the RHS given in previous section, for which the exact solutions are given by Eqs. (25)–(27). For the full von-Kármán system we chose for convenience $\hat{h} = \sqrt{6}$. To monitor the spatial discretization error, we use a time interval of $\Delta\hat{t} = 10^{-5}$ (which produces temporal errors of less than $10^{-10}$), and we plot in Fig. 4 the discrete $L_\infty$ error (as defined in (29)) for the non-dimensional displacement $\hat{w}$ as a function of the space discretization $N$ at the time $\hat{t} = 4$.

Observe the straight line obtained indicating an exponential convergence rate.

We were not able to perform extensive temporal convergence tests with the scheme above for the following reason. For the fixed point method to converge, the solution space is required to have a Lipschitz contraction with a Lipschitz constant which is less than one. We observed through numerical experimentation that in order for this contraction constraint to be met a restriction on the time step was required. Using a space discretization of $N = 13$, and a plate of thickness $\hat{h} = \sqrt{6}$ (as in the problem above), we observed that a time step of $\Delta\hat{t} = 10^{-5}$ was required for the fixed point method to converge. When these conditions were employed, an error of $10^{-10}$ was obtained when examining the discrete $L_\infty$ error of all three

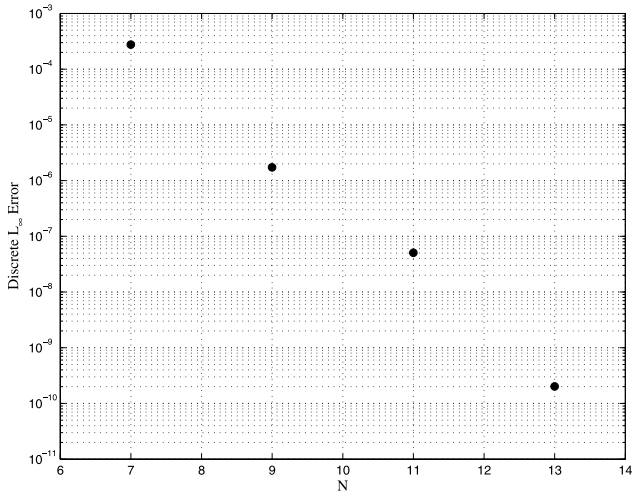


Fig. 4. Discrete $L_\infty$ error for the non-dimensional displacement $\hat{w}(\hat{x}_i, \hat{x}_j, 4)$ versus the number of grid points used per direction in the Chebyshev collocation scheme. Data shown is taken for $\Delta\hat{t} = 10^{-5}$. The full and simplified von-Kármán systems are denoted by circles and squares respectively. The full and simplified von-Kármán solutions overlap.

displacement fields at time $\hat{t} = 4$. Further decrementing the time step did not show any improvement; an attempt to show temporal convergence was futile since the accuracy of exact solution coefficients was no greater than $10^{-10}$. The same time step constraint was found in the case of the simplified von-Kármán system also. The same test as outlined above yielded an error of $10^{-10}$ in all three displacements also.

When using the Newmark-β/fixed point scheme for the von-Kármán system, we observed the following:

- For the full von-Kármán system, the time step restriction imposed by the fixed point iteration seemed to be linearly proportional to the plate thickness. The thinner the plate, the smaller the time step was required for the Lipschitz constant to be less than one.
- No time singularities have been observed which are attributed to inconsistencies in the initial conditions, boundary conditions and uniform forcing as discussed in [15] for the heat equation. The thorough study of this issue is discussed in [16].
- It has been observed that instabilities in time may occur for certain types of discretization of the full von-Kármán system. This is fully explained in [16]. We found that if, at every $M$ steps (where $M$ was determined empirically), we filter the in-plane displacements $\hat{u}$ and $\hat{v}$ using a filtering operator $\mathscr{F}$ defined by:

  $$\mathscr{F}(u(x_i, x_j)) = \tfrac{1}{8}(u(x_{i+1}, x_j) + u(x_{i-1}, x_j) + 4u(x_i, x_j) + u(x_i, x_{j+1}) + u(x_i, x_{j-1})),$$

  where $i, j = 1, \ldots, N-1$, then the scheme converges for all time. A more thorough study of this issue in the context of the von-Kármán system is discussed in [16].

## 5. Numerical examples—controlling discretization errors

The numerical formulation in the previous section is used for solving the full von-Kármán equations (17)–(19) having clamped boundaries according to Eq. (20). For convenience we chose to use $\nu = 0.3$ in our numerical experiments. Spatial and temporal discretization errors are investigated in the following sections.

### 5.1. Spatial discretization

The spatial discretization error is first investigated by examining the non-dimensionalized midpoint deflection after reaching a steady-state, $\hat{w}(1, 1, \hat{t} = 20)$, when a constant load $\hat{g} = 29.6$ is applied, for a plate of thickness $\hat{h} = 0.1$ and $\hat{c} = 1.25$. It is obtained for a $9 \times 9$ grid ($N = 9$) up to $21 \times 21$ grid ($N = 21$), and because an exact solution to the problem is unknown, we present in Fig. 5 the relative difference compared to the midpoint solution obtained with $N = 21$, versus $N$, on a log-linear scale.

$$\text{Relative difference} = \frac{|\hat{w}_N(1, 1, 20) - \hat{w}_{N=21}(1, 1, 20)|}{|\hat{w}_{N=21}(1, 1, 20)|}.$$

The relative difference for all $N$'s lie along a straight line, demonstrating the spectral convergence of the numerical scheme. In all computations presented henceforth we use a grid of $13 \times 13$ points ($N = 13$), where the relative "spatial difference" is seen to be $\approx 2 \times 10^{-4}$.

### 5.2. Temporal discretization

The fixed point method applied in conjunction with the Newmark-β scheme is an iterative method for which a tolerance level has to be specified to determine its convergence and thus terminate the iteration process. As a stopping criterion we examine the discrete $L_\infty$ difference between two successive iterates, and verify that this difference is below a specified tolerance. We first investigate the influence of the tolerance level on the results obtained by taking the tolerance level to be from $10^{-8}$ up to $10^{-11}$. Solving the full

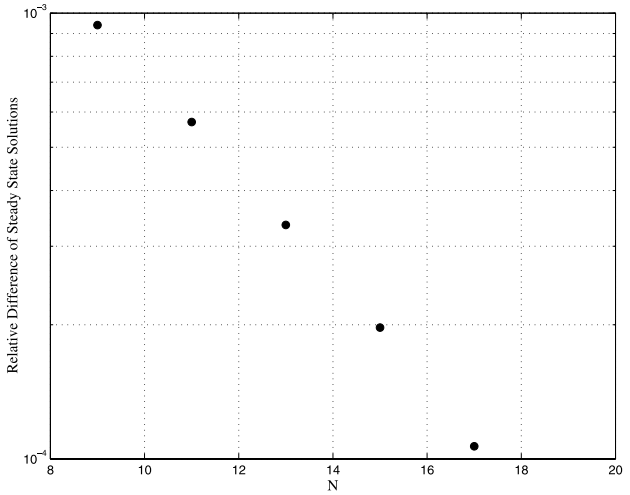


Fig. 5. Relative difference between the steady-state ($\hat{t} = 20$) value of the midpoint displacement $\hat{w}_N(1,1,20)$ for varying spatial resolution $N$ and the midpoint displacement $\hat{w}_{N=21}(1,1,20)$ for $N = 21$. $\Delta t = 10^{-5}$, $\hat{h} = 0.1$, $\hat{c} = 1.25$, $\hat{g} = 29.60$, fixed point convergence tolerance $10^{-10}$, filtering every 1000 time-steps.

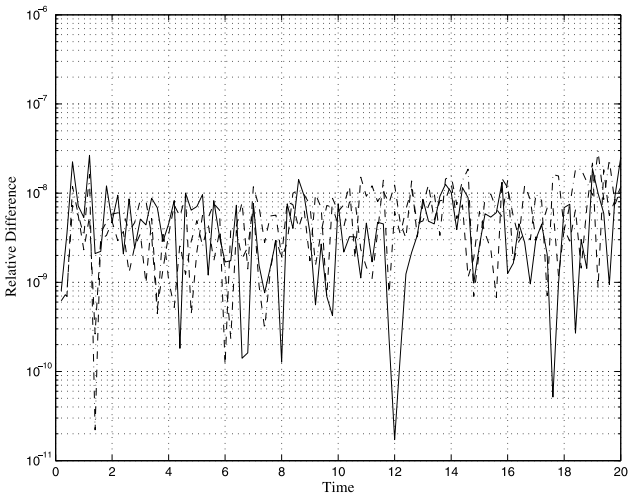


Fig. 6. Time history of the relative difference in the non-dimensional midpoint displacement $\hat{w}$ for different values of the fixed point iteration tolerance. The base line case is a fixed point tolerance of $10^{-11}$. The solid line denotes a tolerance of $10^{-8}$, the dashed line denotes a tolerance of $10^{-9}$ and the dash-dot line denotes a tolerance of $10^{-10}$. $\hat{h} = 0.01$, $N = 13$, $\Delta t = 10^{-6}$, $\hat{c} = 1.25$, $\hat{g} = 29.60$, filtering every 1000 time-steps.

von-Kármán system for a constant load of $\hat{g} = 29.60$, for a plate of thickness $\hat{h} = 0.01$, and a time step of $\Delta t = 10^{-6}$, we present in Fig. 6 the relative difference between $\hat{w}(1,1,\hat{t})$ for each fixed point tolerance level and the solution using a tolerance level of $10^{-11}$.

The maximum relative difference in Fig. 6 is tabulated in Table 1.

Fig. 6 and Table 1 clearly demonstrate that the fixed point tolerance level of $10^{-10}$ suffices, *and is used in all following reported results*.

Table 1
Maximum relative difference between a given fixed point tolerance and a tolerance of $10^{-11}$

| Fixed point tolerance | Maximum relative difference |
|---|---|
| $1.0\times10^{-8}$ | $2.99\times10^{-8}$ |
| $1.0\times10^{-9}$ | $2.81\times10^{-8}$ |
| $1.0\times10^{-10}$ | $3.25\times10^{-8}$ |

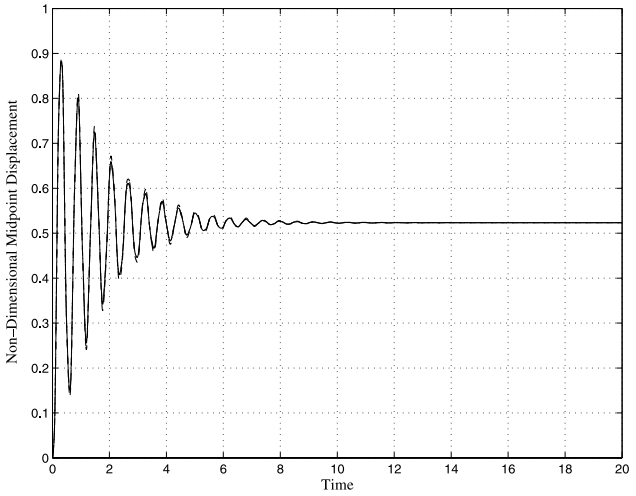


Fig. 7. The midpoint non-dimensional displacement $\hat{w}$ as a function of $\hat{t}$ for different plate thicknesses. Dashed line denotes $\hat{h} = 0.1$, dash-dot line denotes $\hat{h} = 0.01$ and solid line denotes $\hat{h} = 0.001$. $N = 13$, $\Delta t = 10^{-7}$, $\hat{c} = 1.25$, $\hat{g} = 29.60$.

Table 2
Steady-state ($\hat{t} = 20$) non-dimensional midpoint displacement $\hat{w}(1,1,20)$ with varying values of the plate thickness $\hat{h}$. $N = 13$, $\Delta\hat{t} = 10^{-7}$, $\hat{c} = 1.25$, $\hat{g} = 29.60$

| Plate thickness $\hat{h}$ | Steady-state midpoint displacement $\hat{w}$ | Filtering every |
|---|---|---|
| 0.1 | 0.5234888765 | 1000 time-steps |
| 0.01 | 0.5231970397 | 1000 time-steps |
| 0.01 | 0.5234448223 | 100 time-steps |
| 0.001 | 0.5231718713 | 100 time-steps |

To further investigate the temporal discretization error, which is accumulated after each time step, we examine the "steady-state" midpoint non-dimensional deflection (this is taken to be at $\hat{t} = 20$ when $\hat{w}(1,1,\hat{t})$ almost does not change as $\hat{t}$ increases—see Fig. 7) for different time steps used.

*Dynamic solution and the steady-state solution*: The steady-state midpoint non-dimensional solution incorporates both temporal and spatial numerical errors, and may be compared against the static solution available in several references (e.g. [1,3]). Using $\hat{c} = 1.25$, we monitor $\hat{w}$ at the plate midpoint, noticing that for $\hat{t} > 12$ the steady-state is achieved—see Fig. 7.

The numerical values of the steady-state (taken at $\hat{t} = 20$) midpoint non-dimensional displacement for the different plate thicknesses are given in Table 2. In view of Eqs. (17)–(19), the exact steady-state solution should be independent of the plate thickness (this is because $(\hat{h})^2$ multiplies only terms which involve time derivatives). The values in Table 2 do show this trend. The steady-state midpoint displacement serves to quantify numerical errors when compared to static displacements computed using the time independent

von-Kármán equations, as well as modeling errors associated with neglecting terms in the system of equations, and when compared to the fully three-dimensional static solutions (which will be discussed in the next section).

To further quantify the temporal discretization error, we examine the non-dimensional midpoint displacement as $\Delta\hat{t} \to 0$, and its connection to the plate thickness. Although the Newmark-β scheme employed is unconditionally stable for linear problems, due to the fixed point iteration used for the von-Kármán system, one needs to decrease the time step as the plate thickness decreases so that the fixed point iterative scheme converges. As $\Delta\hat{t} \to 0$, we of course expect to obtain $\hat{w}(1,1,\hat{t})$ which tends to a given limit. Examining three different plate thicknesses, i.e. $\hat{h} = 0.1, 0.01, 0.001$, we present $\hat{w}(1,1,\hat{t})$ for $\Delta\hat{t} = 10^{-5}$ up to $\Delta\hat{t} = 10^{-8}$ in Fig. 8.

One may observe that for all $\hat{h}$ the results for the different $\Delta\hat{t}$ are indistinguishable.

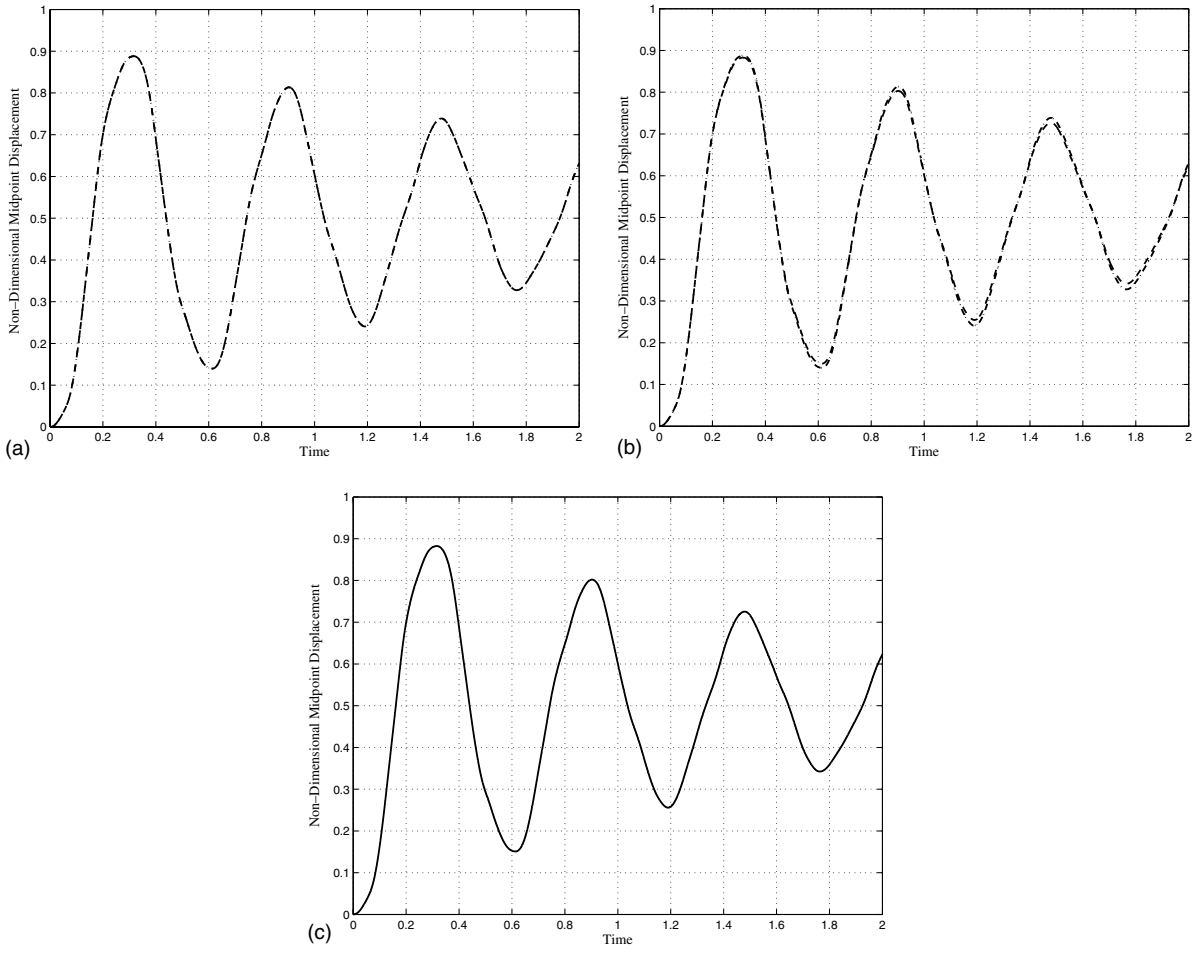


Fig. 8. Time history of the non-dimensional midpoint displacement $\hat{w}(1,1,\hat{t})$ for varying values of plate thickness $\hat{h}$ and time step $\Delta\hat{t}$. $N = 13$, $\hat{c} = 1.25$, $\hat{g} = 29.60$. (a) $\hat{h} = 0.1$, lines-dashed: $\Delta\hat{t} = 10^{-6}$, dash-dot: $\Delta\hat{t} = 10^{-7}$; filter every 1000 steps. (b) $\hat{h} = 0.01$, lines-dashed: $\Delta\hat{t} = 10^{-6}$, dash-dot: $\Delta\hat{t} = 10^{-7}$; filter every 100 steps. (c) $\hat{h} = 0.001$, lines-dash-dot: $\Delta\hat{t} = 10^{-7}$, solid: $\Delta\hat{t} = 10^{-8}$; filter every 100 steps.

## 6. Numerical examples—modeling errors

There are several sources of modeling errors (also known as idealization errors), some of which will be quantified in this section. These are associated with the following assumptions:

(1) Quadratic terms of the form $\partial_i u \partial_j u$ and $\partial_i v \partial_j v$ are negligible with respect to $\partial_1 w \partial_2 w$ in (3). As we shall demonstrate, this assumption is not violated for "reasonable" values of $g$.
(2) The von-Kármán plate model is based on the Kirchhoff–Love displacement field assumption, assumed to be valid for $h/a < 0.07$ and for $w/h < 2$ (see [1, p. 20]). These modeling errors will be quantified by comparing the steady-state solution with the static large-deformation/large-strain three-dimensional elastic solution obtained by $p$-version finite element methods, and to the von-Kármán static solution obtained by [1] using series expansion (believed to be accurate within 2%).

Another modeling assumption further implied is from neglecting the terms associated with time derivatives of $\hat{u}$ and $\hat{v}$ in Eqs. (18) and (19). Neglecting these terms is based on the heuristic assumption that these are negligible (they are of order $\hat{h}^2$) compared to the other order one terms. Examination of the full set of Eqs. (17)–(19), for different $\hat{h} \to 0$ provides a quantitative measure for the heuristic approach, and as will be shown, the heuristic assumption is well justified.

### 6.1. Modeling errors because of neglecting quadratic derivatives of u and v

The derivation of the von-Kármán plate model assumes that quadratic space derivatives of in-plane displacements are negligible with respect to the space derivatives of $w$. To quantify this assumption we consider for example the discrete $L_2$ ratio:

$$R = \frac{\sqrt{\sum_{i=1}^{N}\sum_{j=1}^{N}\left(\left(\partial_1 u(x_{1i},x_{2j})\right)^2 + \left(\partial_2 u(x_{1i},x_{2j})\right)^2\right)}}{\sqrt{\sum_{i=1}^{N}\sum_{j=1}^{N}\left(\left(\partial_1 w(x_{1i},x_{2j})\right)^2 + \left(\partial_2 w(x_{1i},x_{2j})\right)^2\right)}}, \tag{36}$$

and in terms of the non-dimensionalized quantities reads:

$$R = \hat{h}\frac{\sqrt{\sum_{i=1}^{N}\sum_{j=1}^{N}\left(\left(\partial_{\hat{1}}\hat{u}(\hat{x}_{1i},\hat{x}_{2j})\right)^2 + \left(\partial_{\hat{2}}\hat{u}(\hat{x}_{1i},\hat{x}_{2j})\right)^2\right)}}{\sqrt{\sum_{i=1}^{N}\sum_{j=1}^{N}\left(\left(\partial_{\hat{1}}\hat{w}(\hat{x}_{1i},\hat{x}_{2j})\right)^2 + \left(\partial_{\hat{2}}\hat{w}(\hat{x}_{1i},\hat{x}_{2j})\right)^2\right)}}. \tag{37}$$

The ratio $R$ expressed in percentage is examined for the plates with thickness $\hat{h} = 0$ and 0.01 and is plotted in Fig. 9 as the loading $\hat{g}$ is increased for the steady-state solution ($\hat{t} = 20$).

As noticed, the quadratic terms of in-plane spatial derivatives of $u$ are indeed negligible compared to the quadratic spatial derivative of the deflections $w$, thus this modeling assumption does hold. We performed the same check for spatial derivatives of $v$ compared to $w$, leading to the same conclusions. We may conclude that the von-Kármán model is consistent with respect to the assumptions in (3), introducing an error on the order of less than 1%.

### 6.2. Modeling error because of dimension reduction

In order to quantify modeling errors associated with the Kirchhoff–Love displacement field assumption (dimension reduction modeling errors), we performed a static non-linear elastic analysis of a three-dimensional plate of thickness $\hat{h} = 0.01$, for a loading varying from $\hat{g} = 0$ to 100. The $p$-version finite

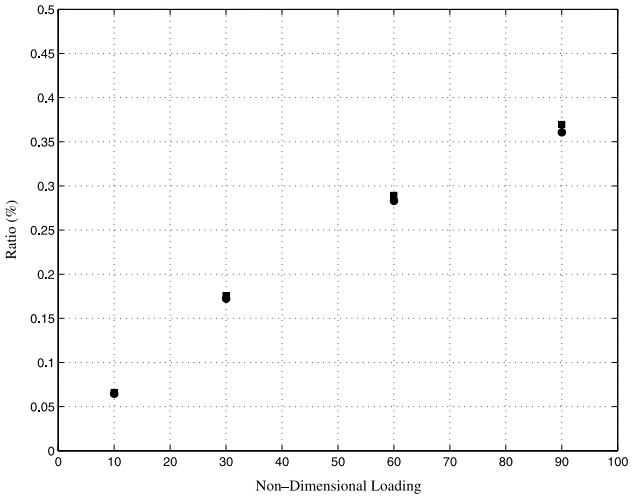


Fig. 9. The $L_2$ discrete ratio (%) for the steady-state solution as defined by (37) versus loading $\hat{g}$. Circles denote $\hat{h} = 0$ and squares denote $\hat{h} = 0.01$. Computation are done with $N = 13$, $\Delta\hat{t} = 10^{-6}$, $\hat{c} = 1.25$, filtering every 100 steps.

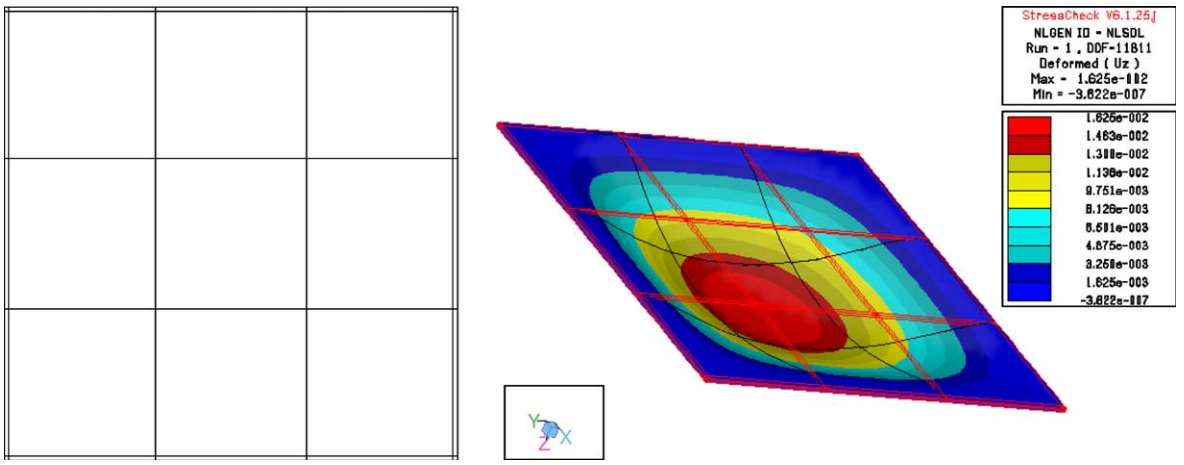


Fig. 10. Three-dimensional $p$-FEM mesh and typical deflection.

element program StressCheck [2] has been used, with a mesh consisting of 50 hexahedral elements, having two layers of elements in the thickness direction, and graded refinements toward the lateral boundaries to account for the boundary layers. The $p$-level has been increased in the linear analysis from 1 to 8 over each element (at $p = 8$ there are close to 1000 degrees of freedom per element) and a non-linear analysis using $p = 8$ has been performed using a tolerance level of 1% in stresses for the non-linear iterative solution. A top-view of the finite element mesh and a typical $w$ displacement is presented in Fig. 10.

[2] StressCheck is trademark of Engineering Software Research and Development, Inc., St. Louis, MO, USA.

The steady-state non-dimensional displacements, the solution of (17)–(19), for plate of thickness $\hat{h} = 0.01$ with $N = 13$, $\Delta t = 10^{-7}$, $\hat{c} = 1.25$, are provided in Fig. 11.

The steady-state non-dimensional displacement obtained by the full von-Kármán system is compared to displacement obtained by the 3-D $p$-FEM analysis for varying loading $\hat{g}$ in Fig. 12. For comparison purposes, we present on same plot the steady-state solutions obtained by other investigators. The steady-state solution of Way presented in [1] is for the static von-Kármán equations, involving no time-derivatives, so it is independent of the plate thickness.

We also solved the simplified von-Kármán system (as if $\hat{h} = 0$), and the steady-state solutions obtained are virtually identical to the full system, as shown in Fig. 12. As clearly visible, the steady-state midpoint displacement $\hat{w}$ agrees very well with this obtained by the 3-D static FE analysis, and the lines are on top of each other so that no difference is observed.

The results of Nath and Kumar are lower compared to those of the 3-D $p$-FEM, and may be attributed to the slight error in their equations (see Remark 4), and a temporal discretization error using a relatively large time step of $8\times10^{-3}$.

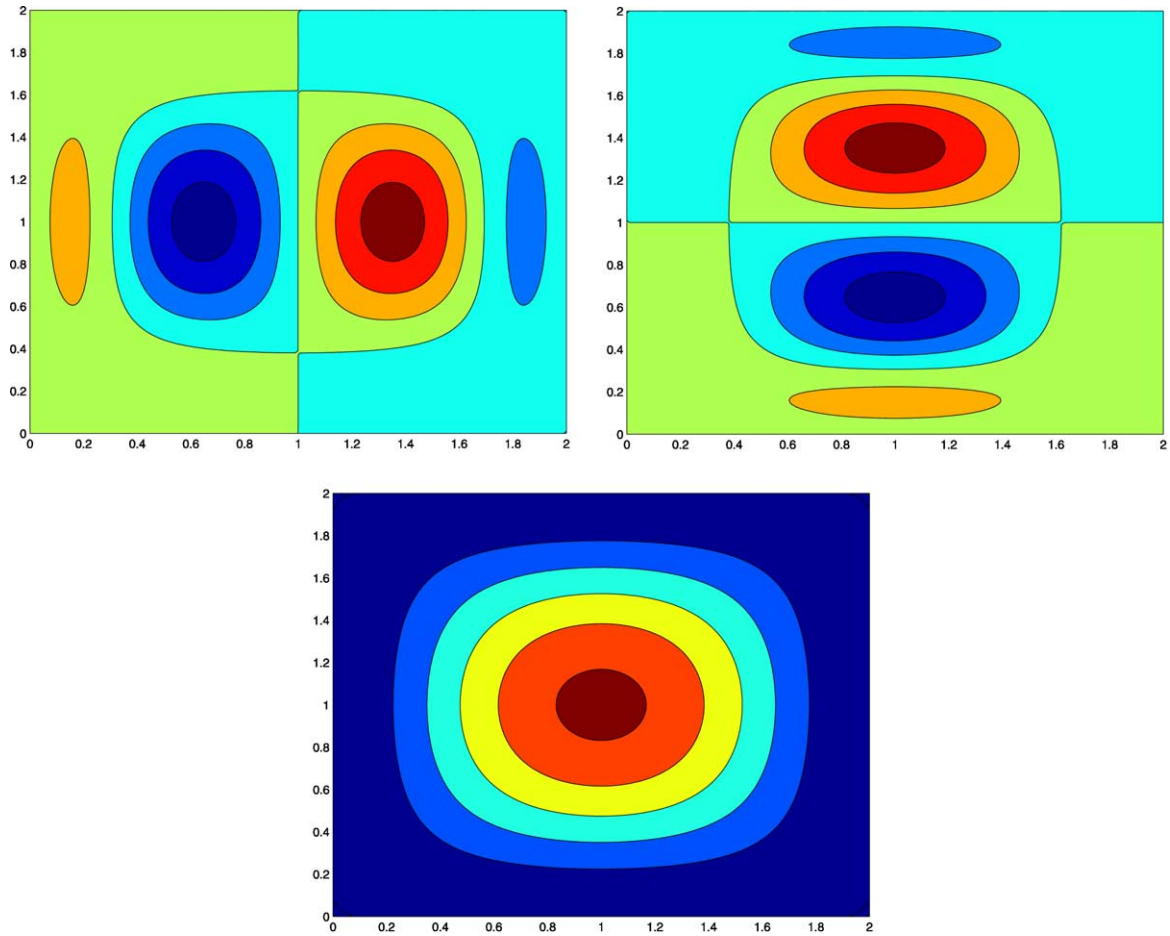


Fig. 11. Steady-state displacement fields $\hat{u}$ (left), $\hat{v}$ (right) and $\hat{w}$ (bottom) for a plate of thickness $\hat{h} = 0.01$. $N = 13$, $\Delta\hat{t} = 10^{-7}$, $\hat{c} = 1.25$, $\hat{g} = 29.60$.

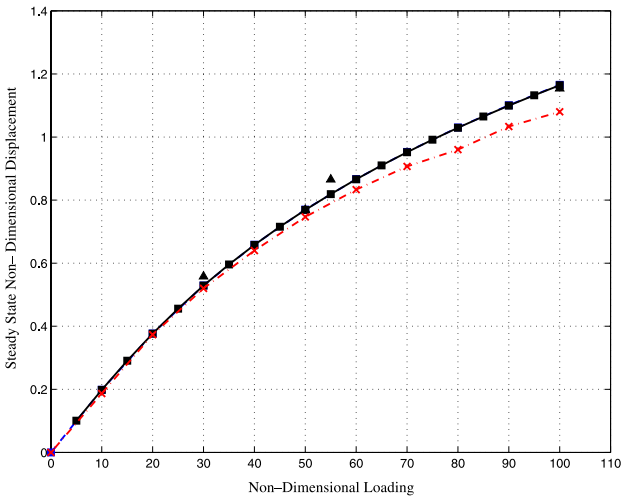


Fig. 12. Steady-state midpoint non-dimensional displacement $\hat{w}$ versus the loading $\hat{g}$. Solid line with circles denotes solution of full and simplified von-Kármán system; Dashed-line with squares denote 3-D $p$-FEM solution—both for $h = 0.01$. Dashed-dot line with $x$s denote the solution of Nath and Kumar [3]; and triangles denote the solution of Way in [1].

### 6.3. Modeling error because of neglecting the in-plane dynamic terms

It is a common assumption in most prior publications addressing the solution of full von-Kármán equations to neglect the in-plane dynamic terms in Eqs. (18) and (19): "*In most engineering application of thin plates...inplane inertial effects can be neglected.*" [1, p. 18], "*...is the assumption that in-plane accelerations $u''$ and $v''$ may be neglected.*" [6, p. 19], "*Neglecting the in-plane and rotary inertia...*" [3]. These are based on the observation that the in-plane dynamic terms are multiplied by the square of the normalized plate thickness, so are considerably small compared to the other terms in Eqs. (18) and (19). However, because von-Kármán is a non-linear system of three equations, the influence of these terms on the solution will be quantified herein.

From the mathematical view point, on the other hand, the full system of dynamic von-Kármán equation, taking into account the in-plane acceleration terms, was considered and global existence and uniqueness of solutions are proven, see e.g. [17] and references therein. These works however do not provide an explicit solution to the von-Kármán system, and one cannot quantify the modeling errors because of neglecting the in-plane dynamic terms.

In view of Eqs. (18) and (19), one may observe that at the limit of $\hat{h} \to 0$, the full system which is solved herein becomes the simplified von-Kármán set. In order to quantify the influence of neglecting these terms, we solve Eqs. (17)–(19) for three different $\hat{h} = 0.1$, 0.01 and 0.001, "freezing" $\hat{g} = 29.60$, $\hat{c} = 1.25$, and discretization parameters: $N = 13$, $\Delta\hat{t} = 10^{-7}$. The time history of the midpoint non-dimensionalized displacement $\hat{w}$, for the three values of plate thickness are plotted in Fig. 13.

One may notice that for plate thicknesses in the range of 0.1 to 0, the influence of the dynamical terms in (18) and (19) is negligible, and the simplified von-Kármán system solution is an excellent approximation to the full von-Kármán system when the deflection is of interest.

To further investigate this type of modeling error, we compare our time dependent solution for $\hat{h} = 0.01$ and 0.001 to that reported by Nath and Kumar [3] (the only time-dependent solution known to us), in which the dynamic in-plane terms are neglected. In our computations the loading is taken to be $\hat{g} = 29.14$ (as reported in [3]), and two different viscosity coefficients are chosen $\hat{c} = 1.25$, 5. The discretization

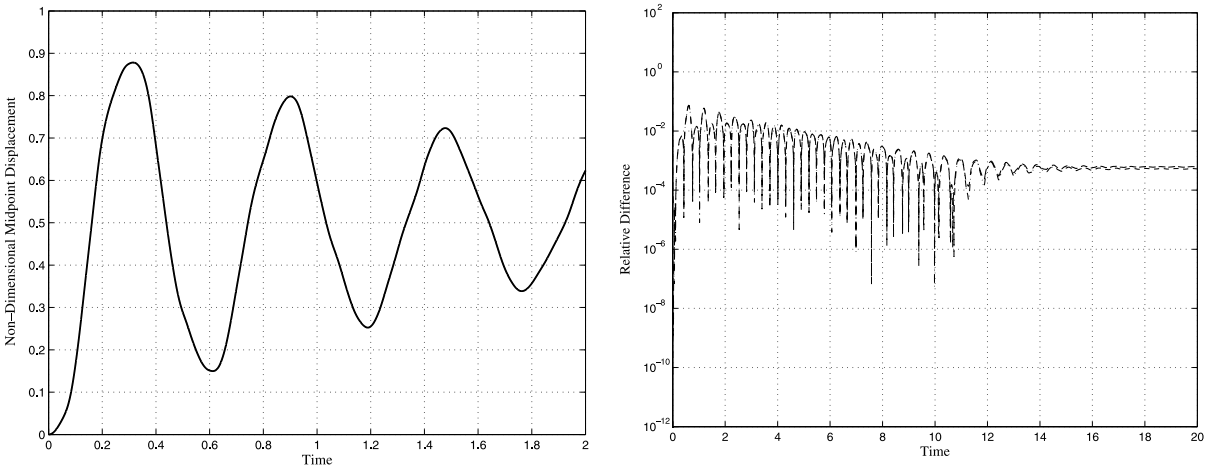


Fig. 13. Time history of the non-dimensional midpoint displacement $\hat{w}$ for varying values of plate thickness $\hat{h}$ (left). Relative differences with respect to $\hat{h} = 0.001$ (right). Dashed line: $\hat{h} = 0.1$, dash-dot line: $\hat{h} = 0.01$ and solid line: $\hat{h} = 0.001$. $N = 13$, $\Delta\hat{t} = 10^{-7}$, $\hat{c} = 1.25$, $\hat{g} = 29.60$.

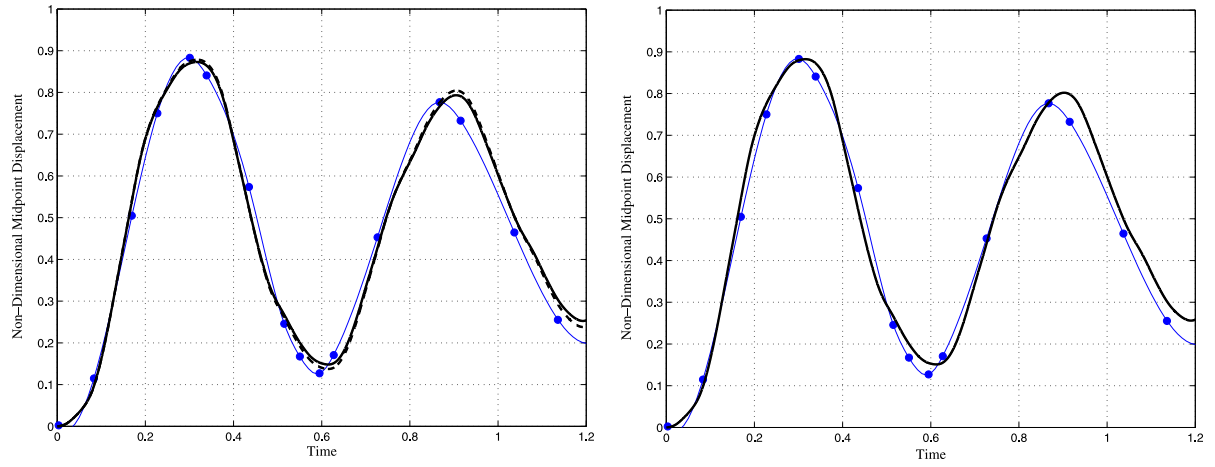


Fig. 14. Time history of the non-dimensional midpoint displacement $w$ versus time for $\hat{c} = 1.25$. Comparing our full von-Kármán solution with that of Nath and Kumar [3]. Blue solid line with circles [3]. Left graph-black dashed line: full von-Kármán solution $\hat{h} = 0.01$, black solid line: $\hat{h} = 0.001$. $N = 13$, $\Delta\hat{t} = 10^{-7}$. Right graph-black solid line: simplified von-Kármán solution $N = 13$, $\Delta\hat{t} = 10^{-6}$.

parameters are $N = 13$, $\Delta\hat{t} = 10^{-7}$. For comparison purposes, we solved also the simplified von-Kármán system. Figs. 14 and 15 present the midpoint non-dimensionalized displacement $\hat{w}$ for $\hat{c} = 1.25$ and 5 respectively.

As anticipated, the full von-Kármán solution for different plate thicknesses are very similar, and close to that reported in [3]. The discrepancies are attributed to the errors in the von-Kármán system in [3] (see Remark 3).

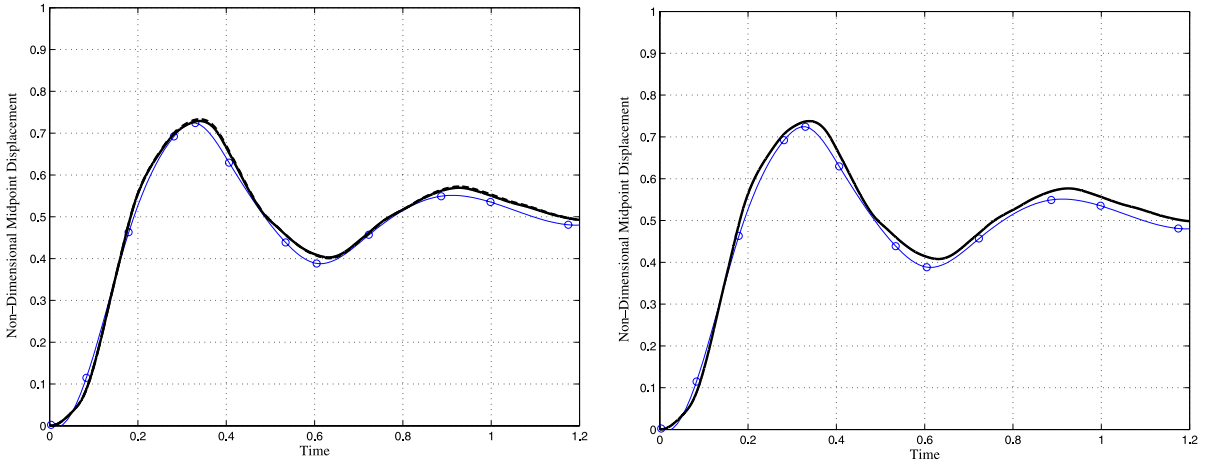


Fig. 15. Time history of the non-dimensional midpoint displacement $w$ versus time for $\hat{c} = 5$. Comparing our full von-Kármán solution with that of Nath and Kumar [3]. Blue solid line with circles [3]. Left graph-black dashed line: full von-Kármán solution $\hat{h} = 0.01$, black solid line: $\hat{h} = 0.01$. $N = 13$, $\Delta\hat{t} = 10^{-7}$. Right graph-black solid line: simplified von-Kármán solution $N = 13$, $\Delta\hat{t} = 10^{-6}$.

### 6.4. Structural viscosity coefficients effects

Another parameter which strongly influences the solution is the structural viscosity coefficient $\hat{c}$. A non-damped ($\hat{c} = 0$) plate is expected to oscillate under an applied constant load indefinitely. To investigate the behavior of the von-Kármán system with respect to the parameter $\hat{c}$, we plot in Fig. 16 the time history of

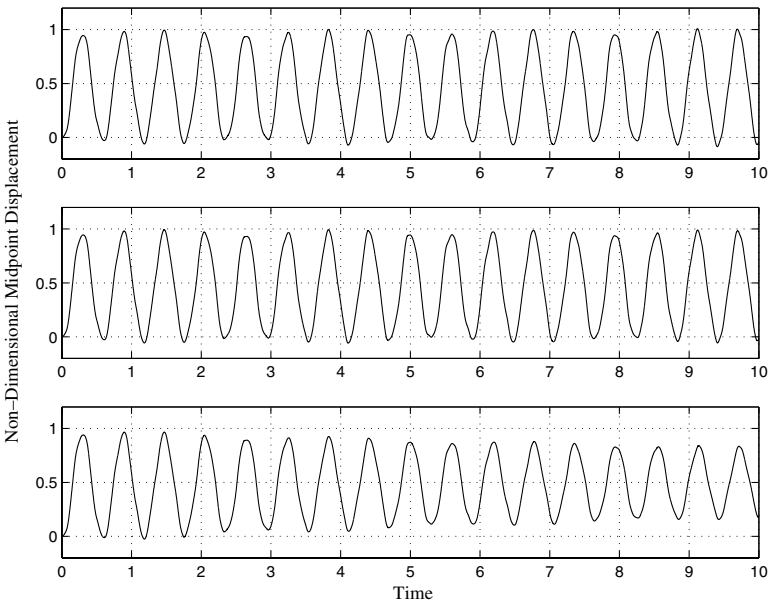


Fig. 16. Time history of the non-dimensional midpoint displacement $\hat{w}$ for different values of structural damping. Top: $\hat{c} = 0$, middle: $\hat{c} = 0.01$, bottom: $\hat{c} = 0.1$. $\Delta\hat{t} = 10^{-6}$, $N = 13$, $\hat{h} = 0.1$.

the non-dimensional midpoint displacement $\hat{w}$ for three different values of structural viscosity coefficients $\hat{c} = 0$, 0.01 and 0.1, for a plate of thickness $\hat{h} = 0.1$.

Indeed for $\hat{c} = 0$ the solution oscillates indefinitely. An interesting observation is the fact that the crests and the troughs are not of constant values, but these have also an oscillatory behavior. This behavior is attributed to the IC/BC incompatibility for a step function constant loading and is investigated further in [16]. As $\hat{c}$ is increased, the oscillation amplitude decreases as expected.

## 7. Summary and conclusions

Herein, the von-Kármán nonlinear, dynamic, partial differential system of three equations, involving fourth order differential operators has been addressed for clamped lateral boundary conditions. Because of our interest in rectangular domains, the system has been discretized using a Chebyshev-collocation method in space and the implicit Newmark-β scheme in time. The pseudo-spectral methods presented can be applied for plates of general geometry using the methods presented in [8,18,19]. Both spatial and temporal discretizations have been rigorously investigated by numerical experimentations, and the discretization errors have been quantified. We have shown by numerical experiments that a spectral convergence rate in space is obtained, and using the fixed point iteration method for solving the Newmark implicit time marching scheme, the spatial discretization error may be controlled as well. Although the Newmark scheme is unconditionally stable and second-order for linear systems, it is well known that due to the non-linearities in our system, a restriction on the time step is necessary so that the fixed point iteration algorithm converges.

Once the discretization errors have been resolved, in the second part of this paper we quantified several sources of idealization errors. We have provided numerical evidence that neglecting quadratic in-plane spatial derivatives and retaining only quadratic spatial derivatives for $\hat{w}$ in the expression of the large-strains is justified. Also, neglecting the dynamic in-plane terms, as done in many previous works, lead to results which are almost identical to the full system for thin, yet finite plate thicknesses.

We have also showed that the steady-state deflections obtained by the von-Kármán system are in excellent agreement compared with these obtained by a three-dimensional high-order non-linear finite elements.

This work has been motivated by a broader research project in which a fluid–structure interaction of a plate embedded in a flow field has to be investigated (see e.g. [4,5]). Towards this end, we have demonstrated that using the simplified von-Kármán system, thus enabling a large time step to be used, is justified and introduces minor modeling errors. Furthermore, several topics mentioned in this paper will be further investigated and reported in a future publication [16], namely: (a) Singularities due to incompatible boundary and initial conditions associated with a constant loading, (b) time instabilities associated with the full von-Kármán system, and its implication on the time-step and filtering restriction and, as a consequence, (c) the necessity to filter the solution.

Other topics as broadening the type of boundary conditions considered to include "pinned" boundary conditions and alike and investigating modeling errors associated with correctly interpreting three-dimensional boundary conditions remains open for future investigation.

## Acknowledgements

The authors thank Prof. George Em Karniadakis of the Division of Applied Mathematics at Brown University, Providence, RI, for helpful discussions, remarks and support, and Dr. Raymond Gordnier of Air Force Research Laboratory, Wright-Patterson AFB, OH, for his comments and help.

The first author gratefully acknowledges the computational support and resources provided by the Scientific Computing and Imaging Institute at the University of Utah, and the useful discussions with Prof. Kris Sikorski of the School of Computing at the University of Utah concerning fixed point contractions.

The second author gratefully acknowledges the support of this work by the Air Force Office of Scientific Research (Computational Mathematics Program) under grant number F49620-01-1-0035.

## References

[1] C.-Y. Chia, Nonlinear analysis of plates, McGraw-Hill, 1980.
[2] W. Han, M. Petyt, Geometrically nonlinear vibration analysis of thin, rectangular plates using the hierarchical finite element method-I: the fundamental mode of isotropic plates, Comput. Struct. 63 (1997) 295–308.
[3] Y. Nath, S. Kumar, Chebyshev series solution to non-linear boundary value problems in rectangular domain, Comput. Methods Appl. Mech. Eng. 125 (1995) 41–52.
[4] R.E. Gordnier, R. Fithen, Coupling of a nonlinear finite element structural method with Navier–Stokes solver. AIAA 2001-2853, 31st Fluid Dynamics Conference, June 2001.
[5] R.E. Gordnier, M.R. Visbal, Development of a three-dimensional viscous aeroelastic solver for nonlinear panel flutter, J. Fluids Struct. 16 (2002) 497–527.
[6] J.E. Lagnese, Boundary stabilization of thin plates, SIAM 1989.
[7] P.G. Ciarlet, Plates and junctions in elastic multi-structures, An asymptotic analysis. RMA 14, Masson/Springer-Verlag, 1990.
[8] C. Canuto, M.Y. Hussaini, A. Quarteroni, T.A. Zang, Spectral Methods in Fluid Mechanics, Springer-Verlag, New York, 1987.
[9] L.N. Trefethen, Spectral Methods in Matlab, SIAM, 2000.
[10] J.L. Humar, Dynamics of Structures, AA Balkema Publishers, 2002.
[11] B.A. Szabó, I. Babuška, Finite Element Analysis, John Wiley & Sons, New York, 1991.
[12] G.E. Karniadakis, S.J. Sherwin, Spectral/*hp* Element Methods for CFD, Oxford University Press, New York, NY, USA, 1999.
[13] R.M. Kirby, Z. Yosibash, Chebyshev-collocation method for bi-harmonic problems with homogeneous Dirichlet boundary conditions, Appl. Num. Math., submitted for publication.
[14] R. Burden, J.D. Faires, Numerical Analysis, PWS Publishing Company, 1993.
[15] N. Flyer, B. Fornberg, Accurate numerical resolution of transients in initial-boundary value problems for the heat equation, J. Comput. Phys. 184 (2003) 526–539.
[16] Z. Yosibash, R.M. Kirby, D. Gottlieb, Collocation methods for the solution of von-Kármán dynamic non-linear plate systems, J. Comput. Phys., submitted for publication.
[17] J.P. Puel, M. Tucsnak, Global existence for the full von-Kármán system, Appl. Math. Optim. 34 (1996) 139–160.
[18] D.A. Kopriva, A spectral multidomain method for the solution of hyperbolic systems, Appl. Num. Math. 2 (1986) 221–241.
[19] D.A. Kopriva, Computation of hyperbolic equations on complicated domains with patched and overset Chebyshev grids, SIAM J. Sci. Stat. Comput. 10 (1989) 120–132.